3.3 DOUBLY CURVED SHELLS.

Doubly curved shells are frequently used in space vehicles as external closures of fuel tanks or entry vehicles or an internal common bulkheads. When doubly curved shells develop compressive membrane forces in reaction to externally applied loads, their load-carrying capacity is often limited by structural instability, or buckling.

The buckling strength of a doubly curved shell depends upon its curvature, its geometric proportions (including the stiffening, when present), the elastic properties of its materials, the manner in which its edges are supported, and the nature of the applied loading. Initial, although small, geometric deviations of the shell from its ideal shape can have a significant adverse effect on the buckling strength of doubly curved shells and can cause large scatter of experimental results.

This paragraph recommends practices for design of compressively loaded doubly curved shells. Included are practices recommended for the design of complete spheres, ellipsoids, and toroids, as well as bulkheads. Most of the data are for shells subjected to uniform pressure loads, although data are also given for point loads on spheres.

The reduction of critical buckling loads caused by imperfections, small dynamic oscillations, boundary conditions, and the like is usually accounted for by multiplying the theoretical buckling loads by a correlation factor to obtain a lower-bound conservative estimate. However, when insufficient data are available to obtain correlation factors, testing is recommended to verify the design. Experimental verification is also recommended for shells of arbitrary shape and for shells of revolution having cutouts, joints, plasticity effects, and nonuniform shell stiffness. The effect of small oscillations in applied loading is considered to be accounted for by the correlation factor.

For doubly curved shells, considerable capability for theoretical analysis is available although experimental investigations of the stability of doubly curved shells lag far behind analytical capabilities; the shallow spherical cap under external pressure is the only problem which has been investigated extensively.

The growing use of digital computers for analysis of shell structures has greatly improved the available analyses which can be performed. For example, a comprehensive computer program, BOSOR 3, [1] performs a stability analysis of segmented, ring-stiffened shells of revolution. The program is quite general with respect to types of loading, geometry, boundary conditions, and wall stiffness variation. All the programs for doubly curved shells, including both finite-difference and finite-element, treat only those cases in which the shell does not become plastic before buckling.

Although the capability for stability analysis has increased, parametric optimization studies for problems of interest are lacking. This may well be because of the relative newness of most computer programs. To date, most computer programs have been used for spot checks of approximate solutions and for comparisons with experimental data.

The designer is advised to be alert to new developments in shell-stability analysis.

3.3.1 ISOTROPIC DOUBLY CURVED SHELLS.

Unstiffened isotropic doubly curved shells subjected to various conditions of loadings are considered in this paragraph. Solutions are limited to spherical, ellipsoidal, and toroidal shells.

3.3.1.1 Spherical Caps Under Uniform External Pressure.

The buckling of a spherical cap under uniform external pressure (Fig. 3.3-1) has been treated extensively. The theoretical results are presented in References 2 and 3 for axisymmetric snap-through of shallow spherical

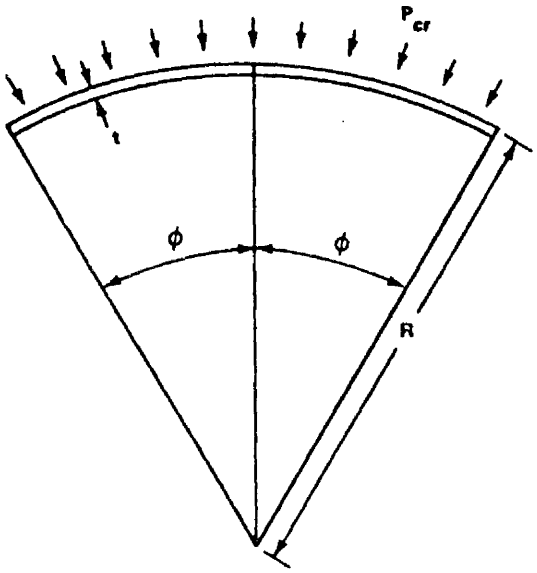

FIGURE 3.3-1. GEOMETRY OF SPHERICAL CAP UNDER UNIFORM EXTERNAL PRESSURE

shells with edges that are restrained against translation but are either free to rotate or are clamped. Results for asymmetric buckling are given in References 4 and 5 for the same boundary conditions. The results reported in these references are presented as the ratio of the buckling pressure p_{cr} for the spherical cap and the classical buckling pressure $p_{c\ell}$ for a complete spherical shell as a function of a geometry parameter λ :

$$\frac{p_{cr}}{p_{c\ell}} = f(\lambda) \qquad (1)$$

with

$$p_{c\ell} = \frac{2}{[3(1-\mu^2)]^{1/2}} \; E\left(\frac{t}{r}\right)^2 \quad , \qquad (2)$$

$$\lambda = [12(1-\mu^2)]^{1/4} \; (R/t)^{1/2} \; 2 \sin\frac{\phi}{2} \qquad (3)$$

where ϕ is half the included angle of the spherical cap (Fig. 3.3-1). The function $f(\lambda)$ depends on the boundary conditions imposed on the shell.

Most of the available test data apply to spherical shells, and the values are lower than the theoretically predicted buckling pressures. The discrepancy between theory and experiment can be attributed largely to initial deviations from the ideal spherical shape [3, 6, 7] and to differences between the actual and assumed edge conditions [8, 9]. Most of the available data are

summarized in Reference 10; some other test results are given in References 6 and 11. A lower bound to the data for clamped shells is given by

$$\frac{p_{cr}}{p_{cl}} = 0.14 + \frac{3.2}{\lambda^2} \quad (\lambda > 2) \qquad . \qquad (4)$$

This curve is plotted in Figure 3.3-2. Whereas the λ parameter is used in shallow-shell analysis, Figure 3.3-2 may be applied to deep shells as well as to shallow shells.

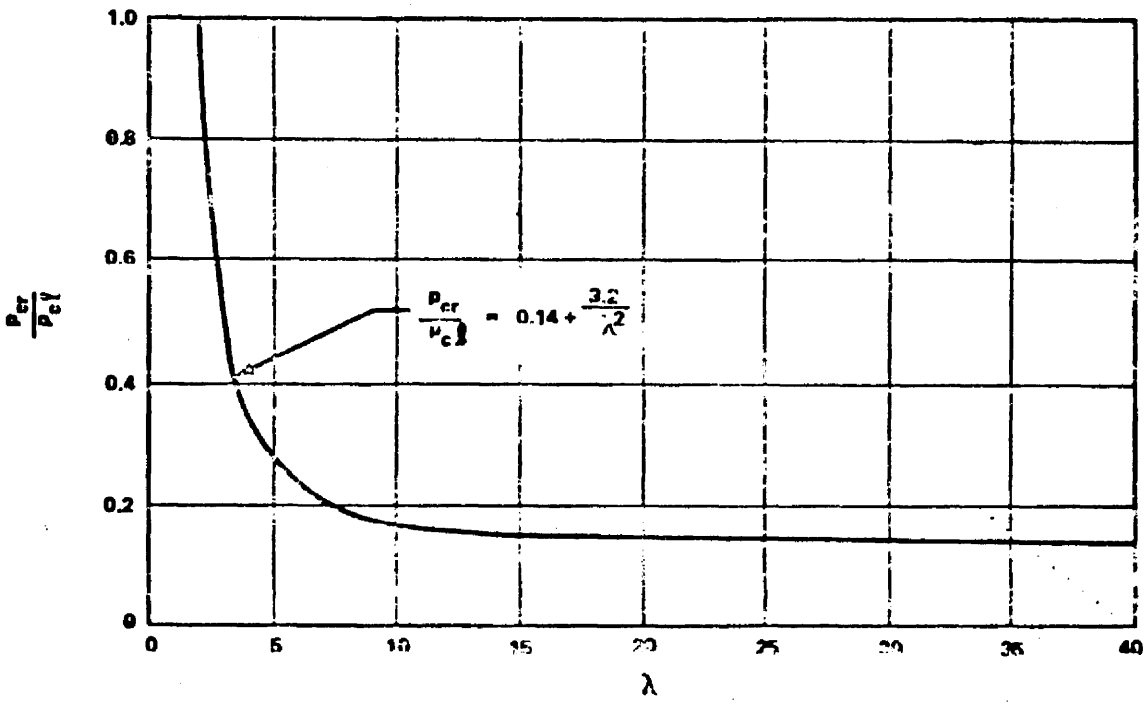

FIGURE 3.3-2. RECOMMENDED DESIGN BUCKLING PRESSURE OF SPHERICAL CAPS

3.3.1.2 Spherical Caps Under Concentrated Load at the Apex.

Spherical caps under concentrated load at the apex (Fig. 3.3-3) will buckle under certain conditions. The theoretical results for edges that are free to rotate and to expand in the direction normal to the axis of revolution,

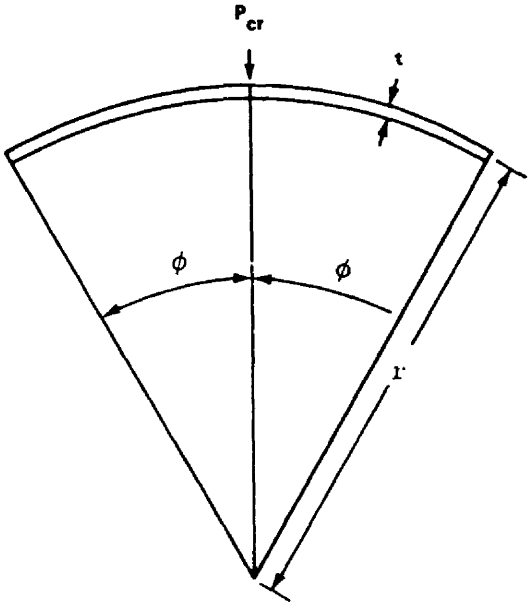

FIGURE 3.3-3. GEOMETRY OF SPHERICAL CAP UNDER CONCENTRATED LOAD AT THE APEX

and for clamped edges, are given in Reference 12 for axisymmetric snap-through and in References 13 and 14 for asymmetric buckling. Experimental results for loads which approximate concentrated loading are described in References 15 to 19.

For shells with unrestrained edges, buckling will not occur if λ is less than about 3.8. In this range of shell geometry, deformation will increase with increasing load until collapse resulting from plasticity effects occurs. For shells with values of λ greater than 3.8, theoretical and experimental results are in good agreement for axisymmetric snap-through but disagree when theory indicates that asymmetric buckling should occur first. In this case, buckling and collapse are apparently not synonymous, and only collapse loads have been measured. A lower-bound relationship between the collapse-load parameter and the geometry parameter for the data of References 13, 15, and 16 for shells with unrestrained edges is given by

$$\frac{P_{cr}\, r}{Et^3} = \frac{1}{24}\,\lambda^2 \quad (4 \le \lambda \le 18) \qquad . \qquad (5)$$

For spherical caps with clamped edges, theory indicates that buckling will not occur if λ is less than about 8. For values of λ between 8 and 9, axisymmetric snap-through will occur, with the shell continuing to carry an increasing load. For larger values of λ, asymmetrical buckling

will occur first, but the shell will continue to carry load. Although imperfections influence the initiation of symmetric or asymmetric buckling, few measurements have been made of the load at which symmetric or asymmetric deformations first occur. Experimental results indicate that the collapse loads of clamped spherical caps loaded over a small area are conservatively estimated by the loads calculated in Reference 13 and shown in Figure 3.3-4. When the area of loading becomes large, large buckling may occur at a lower level.

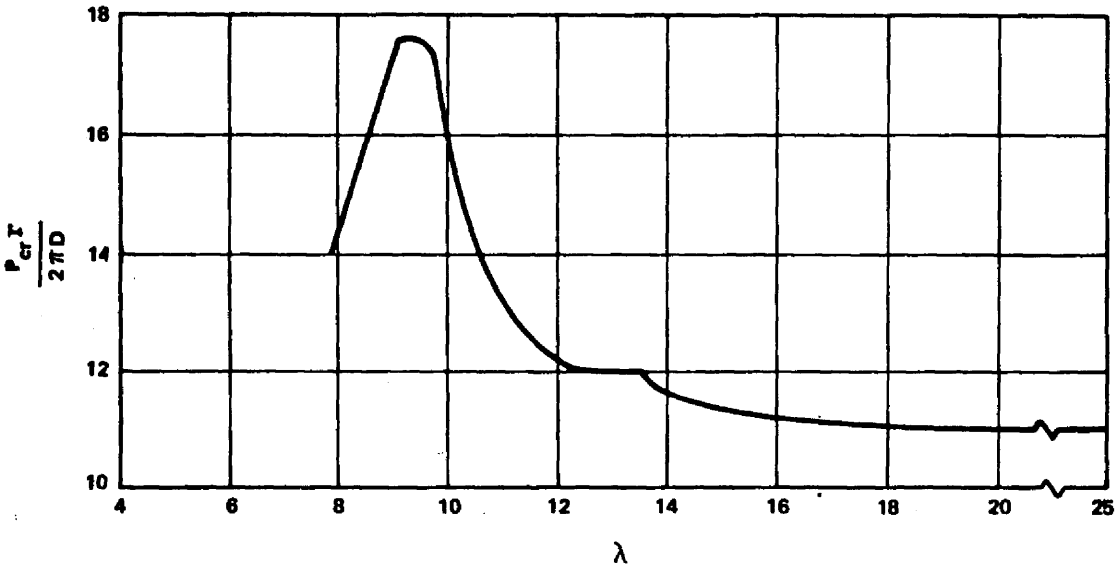

FIGURE 3.3-4. THEORETICAL BUCKLING LOADS FOR CLAMPED SPHERICAL CAP UNDER CONCENTRATED LOAD

3.3.1.3 Spherical Caps Under Uniform External Pressure and Concentrated Load at the Apex.

Clamped spherical caps subjected to combinations of uniform external pressure and concentrated load at the apex are discussed in Reference 20. The experimental and theoretical data given there are insufficient, however,

to yield conclusive results. A straight-line interaction curve is recommended:

$$\frac{P}{P_{cr}} + \frac{p}{p_{cr}} = 1 \qquad (6)$$

where P is the applied concentrated load, p is the applied uniform pressure, P_{cr} the critical concentrated load given in Paragraph 3.3.1.2, and p_{cr} the critical uniform external pressure given in Paragraph 3.3.1.1.

3.3.1.4 Complete Ellipsoidal Shells Under Uniform External Pressure.

Ellipsoidal shells of revolution subjected to uniform external pressure, as shown in Figure 3.3-5, are treated in Reference 21. Calculated theoretical results for prolate spheroids are shown in Figures 3.3-6a and 3.3-6b. Experimental results given in Reference 22 for prolate spherical shells with $4 > A/B > 1.5$ are in reasonably close agreement with the theoretical results of Reference 21. For $A/B \geq 1.5$, the theoretical pressure should be multiplied by the factor 0.75 to provide a lower bound to the data. The results given in Reference 23 for half of a prolate spheroidal shell $(A/B = 3)$ closed by an end plate are in good agreement with those for the complete shell.

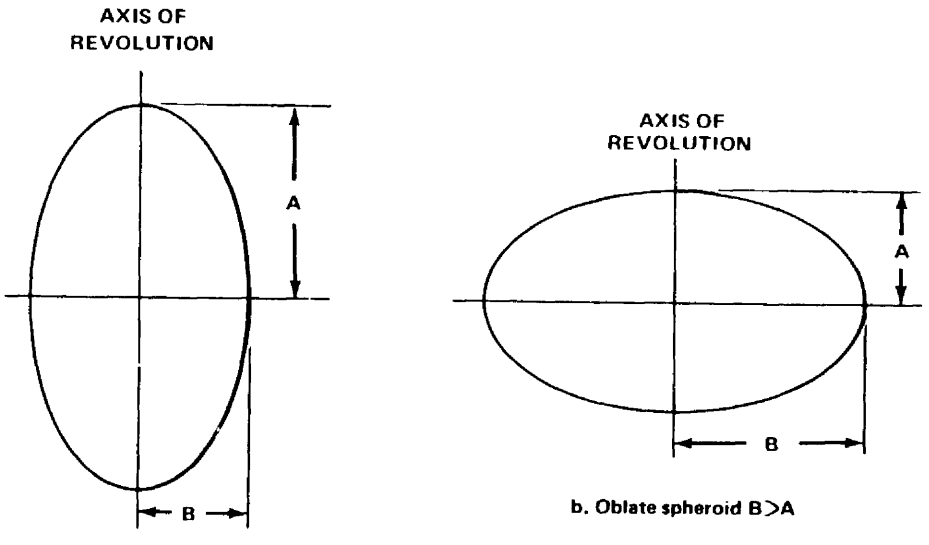

a. Prolate spheroid A>B

b. Oblate spheroid B>A

FIGURE 3.3-5. GEOMETRY OF ELLIPSOIDAL SHELLS

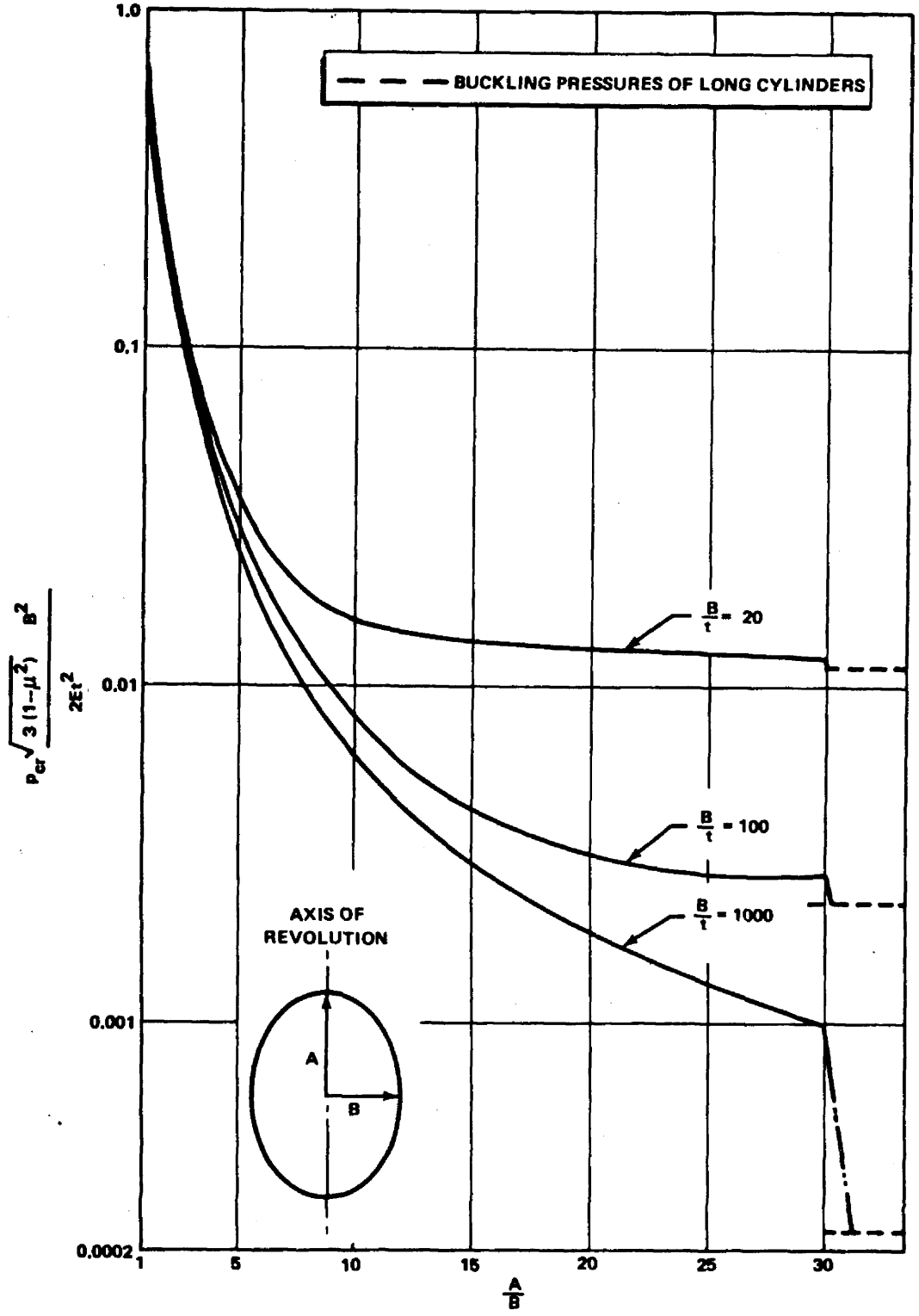

FIGURE 3.3-6a. THEORETICAL EXTERNAL BUCKLING PRESSURES OF PROLATE SPHEROIDS ($\mu = 0.3$)

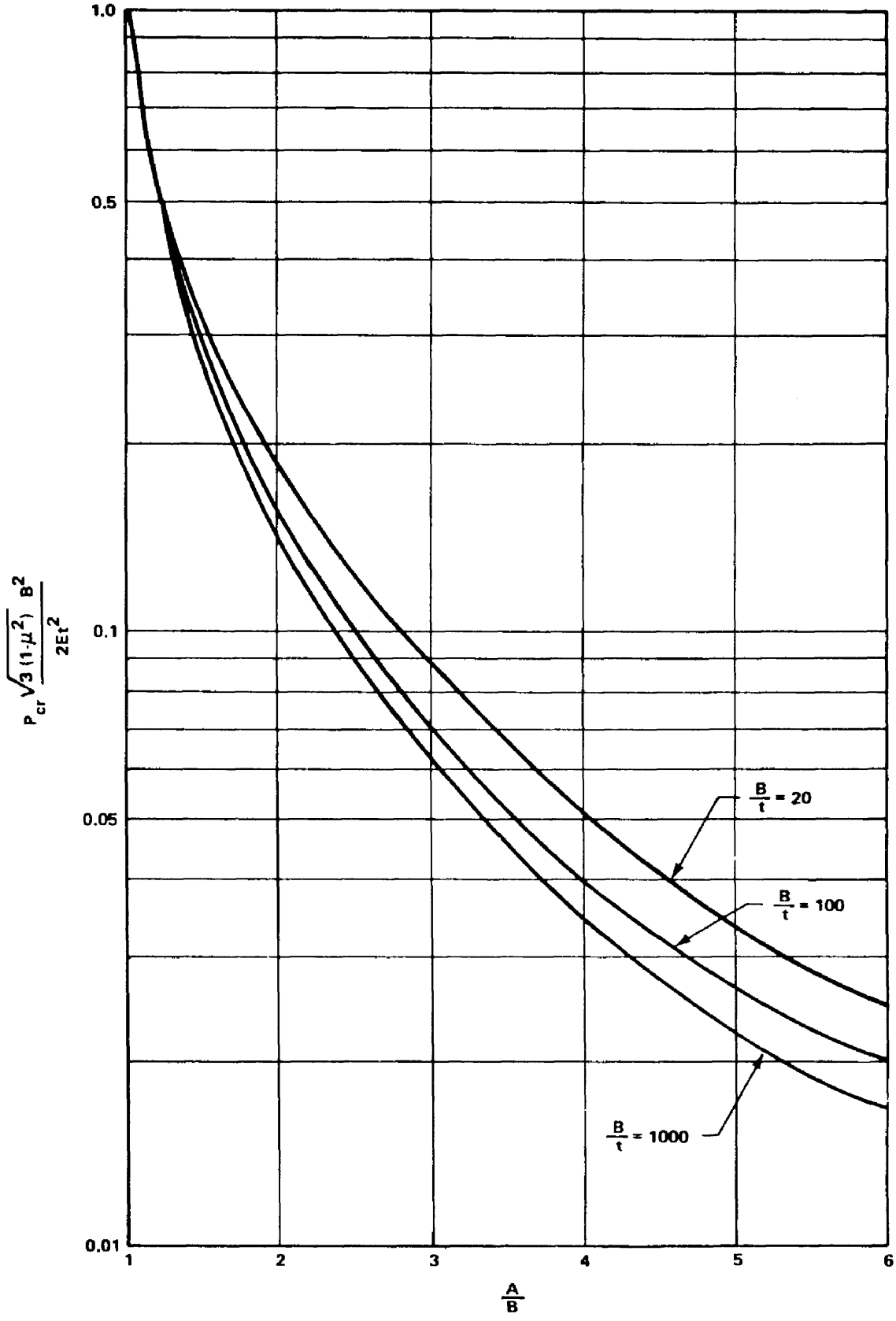

FIGURE 3.3-6b. THEORETICAL EXTERNAL BUCKLING PRESSURES OF PROLATE SPHEROIDS ($\mu = 0.3$) FOR A/B RATIO OF 1:6

The analysis of Reference 21 indicates that theoretical results for thin, oblate spheroidal shells are similar to those for a sphere of radius

$$R_A = \frac{B^2}{A} \quad . \tag{7}$$

The data of Reference 24 show that the experimental results are similar as well. Thus, the external buckling pressure for a thin, oblate spheroid may be approximated by the relationship

$$\frac{\sqrt{3\,(1-\mu^2)}}{2}\left(\frac{R_A}{t}\right)^2 \frac{p}{E} = 0.14 \quad , \tag{8}$$

which is the limit of equation (4) as λ becomes large.

3.3.1.5 Complete Oblate Spheroidal Shells Under Uniform Internal Pressure.

When the ratio A/B of an oblate spheroid is less than $\sqrt{2}/2$, internal pressure produces compressive stresses in the shell, and hence allows instability to occur. The theoretical values of the critical internal pressures given by the analysis of Reference 21 are shown in Figure 3.3-7. No experimental results are available, but the study of the imperfection sensitivity of Reference 21 indicates that there should be good agreement between theory and experiment for shells with $0.5 < A/B < 0.7$.

3.3.1.6 Ellipsoidal and Torispherical Bulkheads Under Internal Pressure.

Clamped oblate spheroidal (ellipsoidal) bulkheads (Fig. 3.3-8) may have the ratio of length of minor and major axes (A/B) less than $\sqrt{2}/2$ without buckling under internal pressure, provided that the thickness exceeds a certain critical value. This problem is investigated in Reference 25.

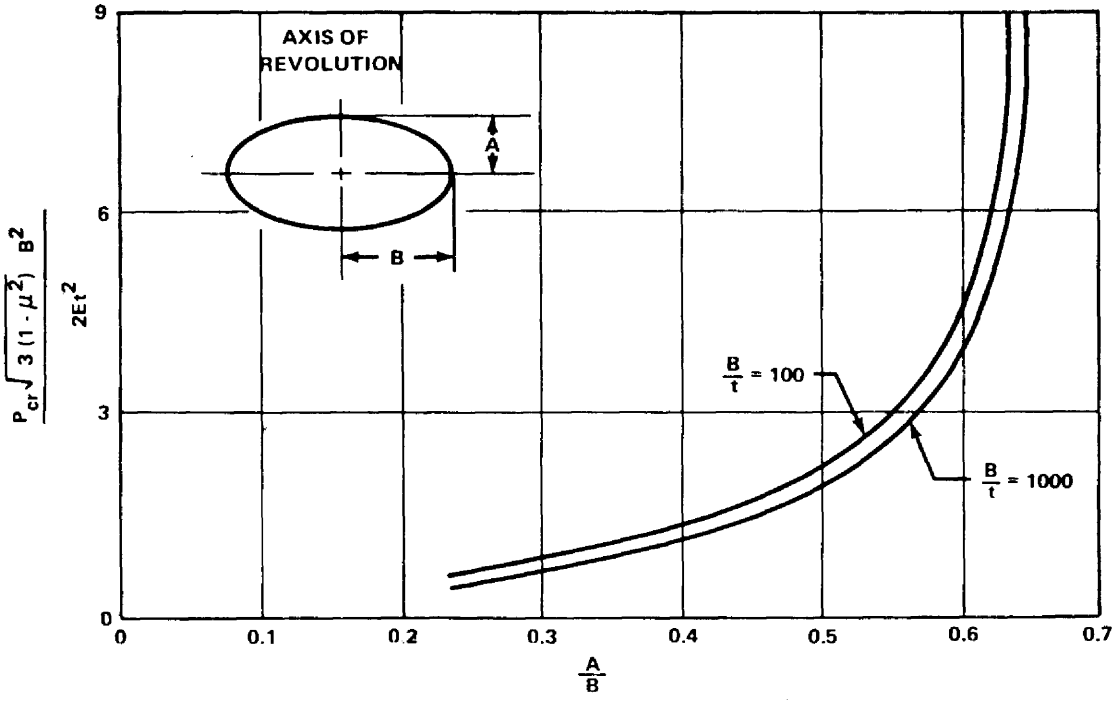

FIGURE 3.3-7. THEORETICAL BUCKLING PRESSURES OF OBLATE SPHEROIDS UNDER INTERNAL PRESSURE ($\mu = 0.3$)

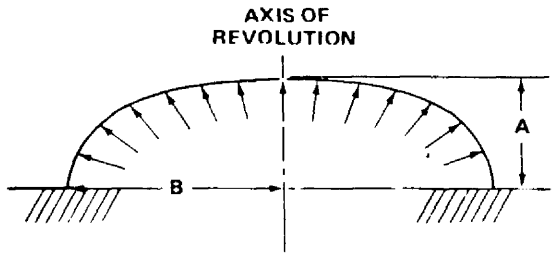

FIGURE 3.3-8. CLAMPED ELLIPSOIDAL BULKHEAD UNDER INTERNAL PRESSURE

A nonlinear bending theory is used to determine the prebuckling stress distribution. The regions of stability are shown in Figure 3.3-9; the calculated variation of buckling pressure with thickness is shown in Figure 3.3-10. The theory has not been verified by experimental results, however, and should be used cautiously.

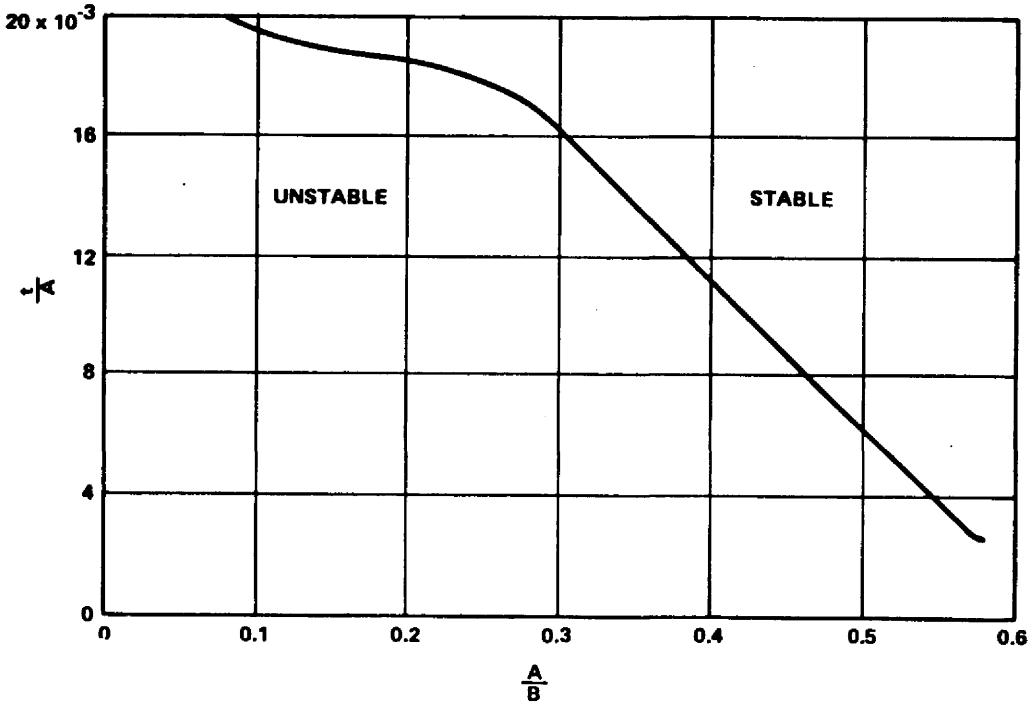

FIGURE 3.3-9. REGION OF STABILITY FOR ELLIPSOIDAL CLOSURES SUBJECTED TO INTERNAL PRESSURE ($\mu = 0.3$)

Torispherical end closures (Fig. 3.3-11) are also investigated in Reference 25. Calculations are made for the prebuckling stress distribution in these bulkheads for ends restrained by cylindrical shells and for buckling pressures for torispherical bulkheads with clamped edge conditions after buckling. The results are shown in Figure 3.3-12. The experimental results of Reference 26 indicate that the theoretically predicted buckling pressures should be multiplied by a correlation factor γ equal to 0.7.

3.3.1.7 Complete Circular Toroidal Shells Under Uniform External Pressure.

The complete circular toroidal shell under uniform external pressure (Fig. 3.3-13) has been investigated and is described in Reference 27; the theoretical results obtained are shown in Figure 3.3-14.

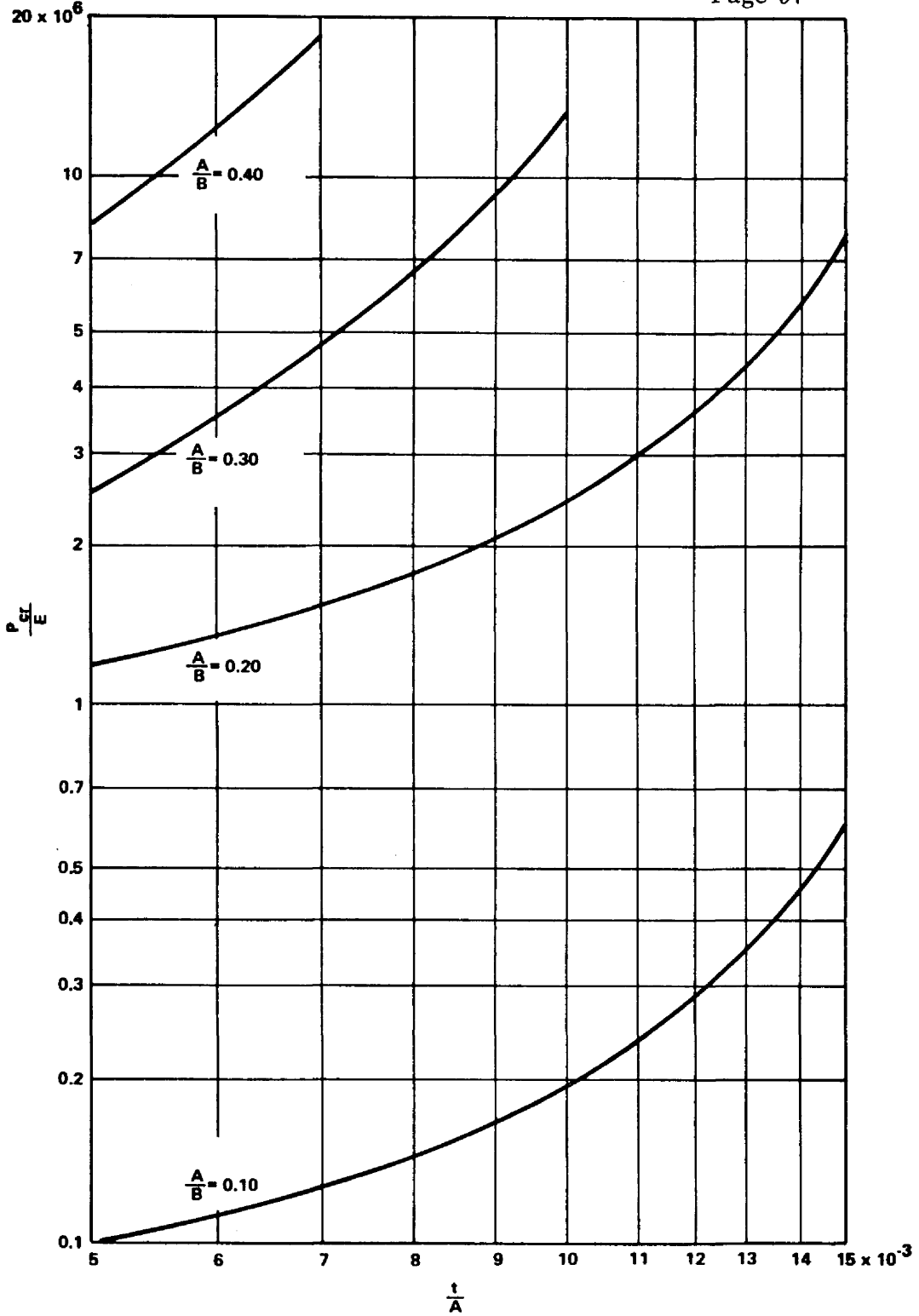

FIGURE 3.3-10. THEORETICAL RESULTS FOR CLAMPED ELLIPSOIDAL BULKHEADS SUBJECTED TO UNIFORM INTERNAL PRESSURE ($\mu = 0.3$)

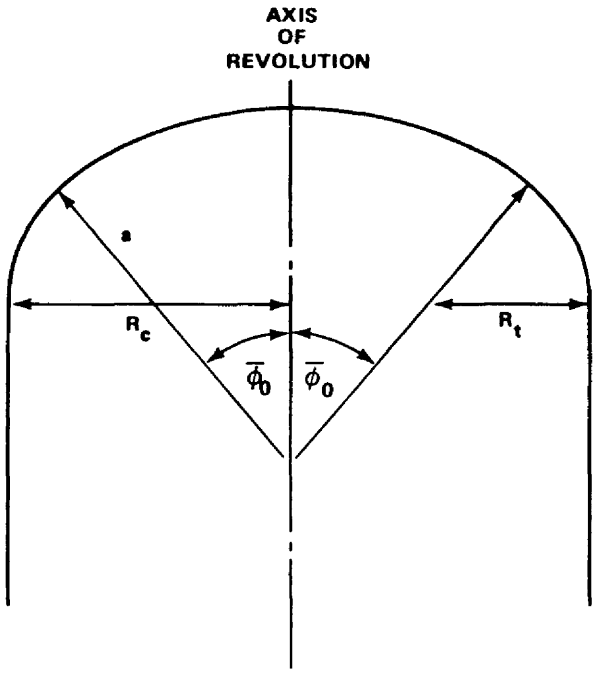

FIGURE 3.3-11. GEOMETRY OF TORISPHERICAL CLOSURE

The experimental results are given in Reference 27 for values of b/a of 6.3 and 8 and indicate good agreement with theory. For values of b/a equal to or greater than 6.3, the theoretical buckling pressure should be multiplied by a factor of 0.9 to yield design values. This correction factor has been recommended in Reference 28 for long cylindrical shells which correspond to a value of b/a of ∞. For values of b/a less than 6.3, the buckling pressure should be verified by test.

3.3.1.8 Shallow Bowed-Out Toroidal Segments Under Axial Loading.

A bowed-out equatorial toroidal segment under axial tension (Fig. 3.3-15) will undergo compressive circumferential stress and will thus be susceptible to buckling. An analysis for simply supported shallow segments is given in Reference 29 and yields the relationship

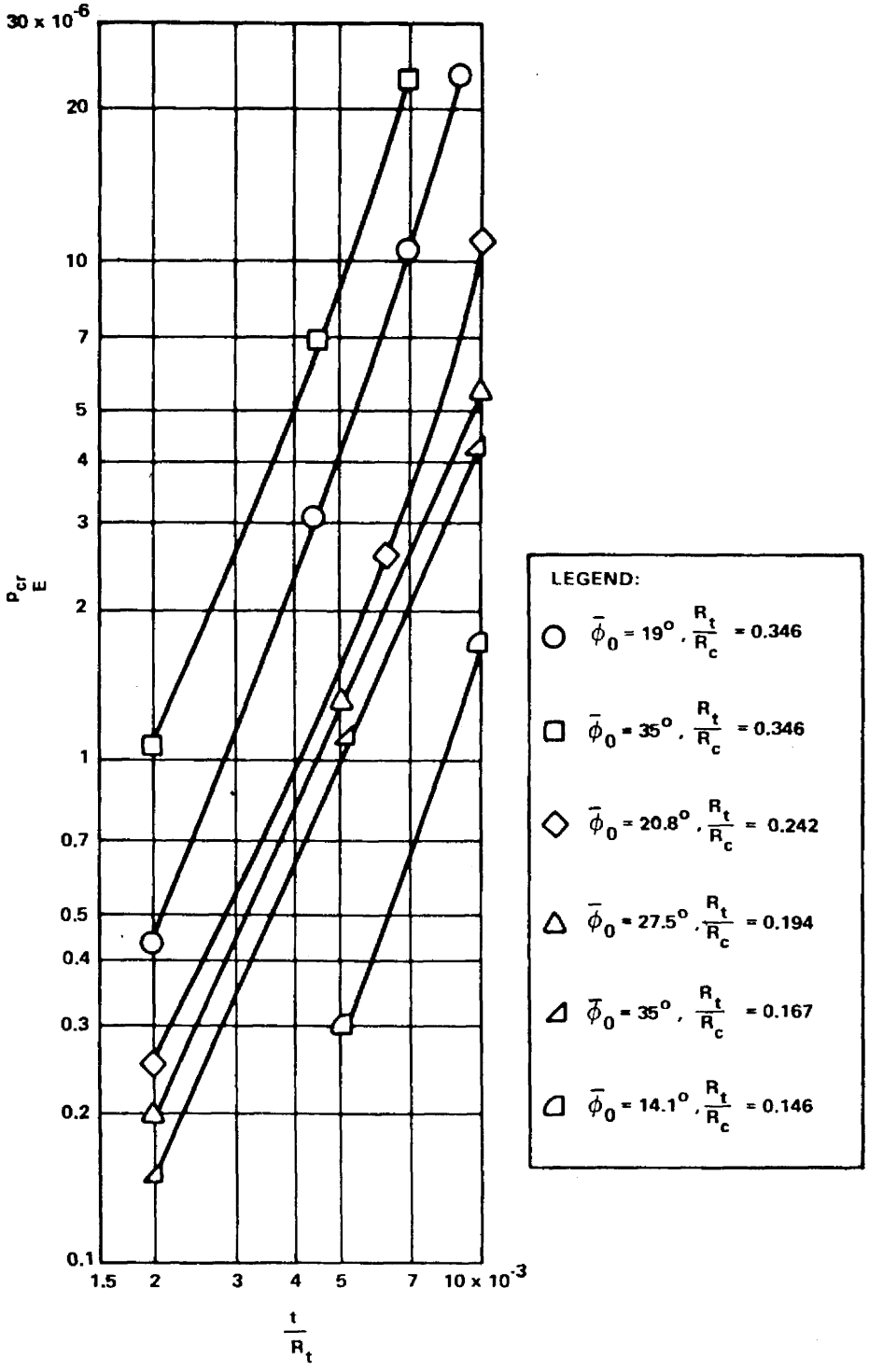

FIGURE 3.3-12. THEORETICAL RESULTS FOR TORISPHERICAL CLOSURES SUBJECTED TO UNIFORM INTERNAL PRESSURE ($\mu = 0.3$)

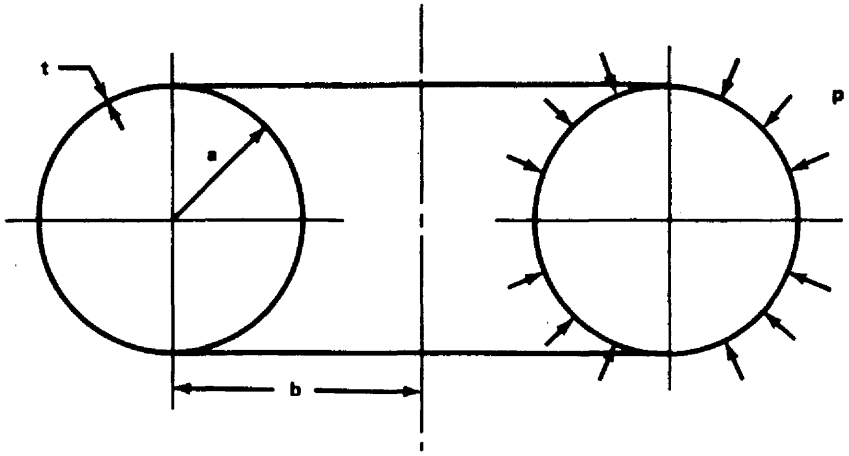

FIGURE 3.3-13. GEOMETRY OF A TOROIDAL SHELL UNDER UNIFORM EXTERNAL PRESSURE

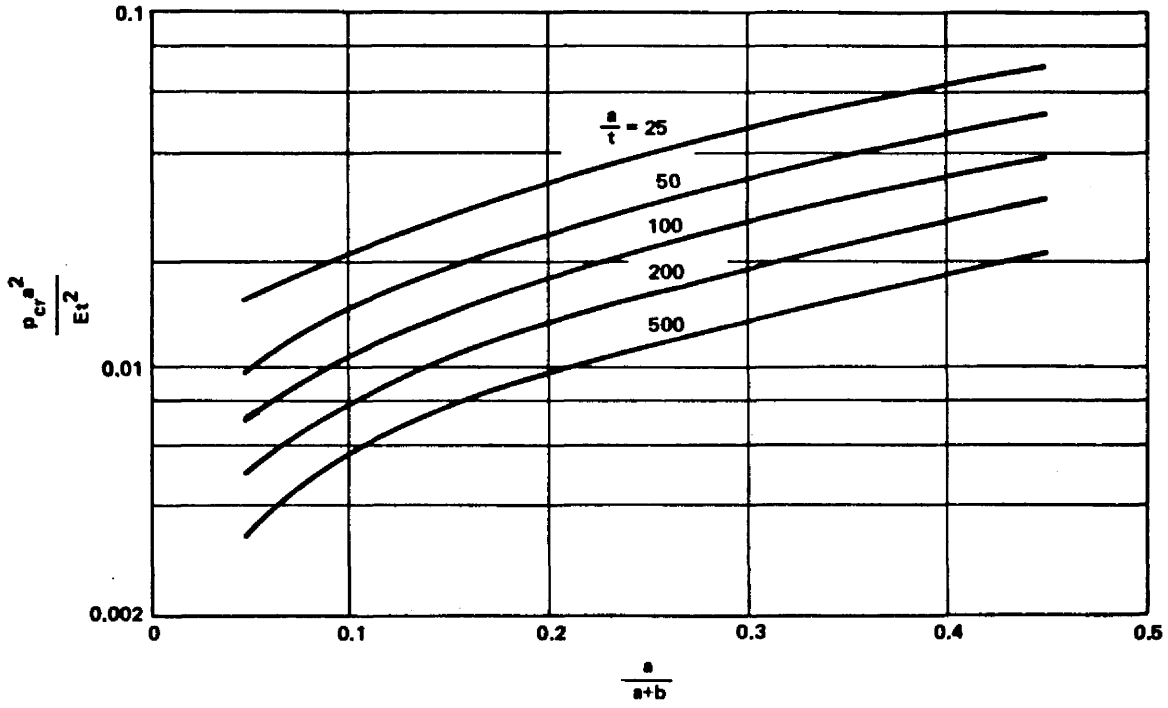

FIGURE 3.3-14. THEORETICAL BUCKLING COEFFICIENTS FOR TOROIDAL SHELLS UNDER UNIFORM EXTERNAL PRESSURE

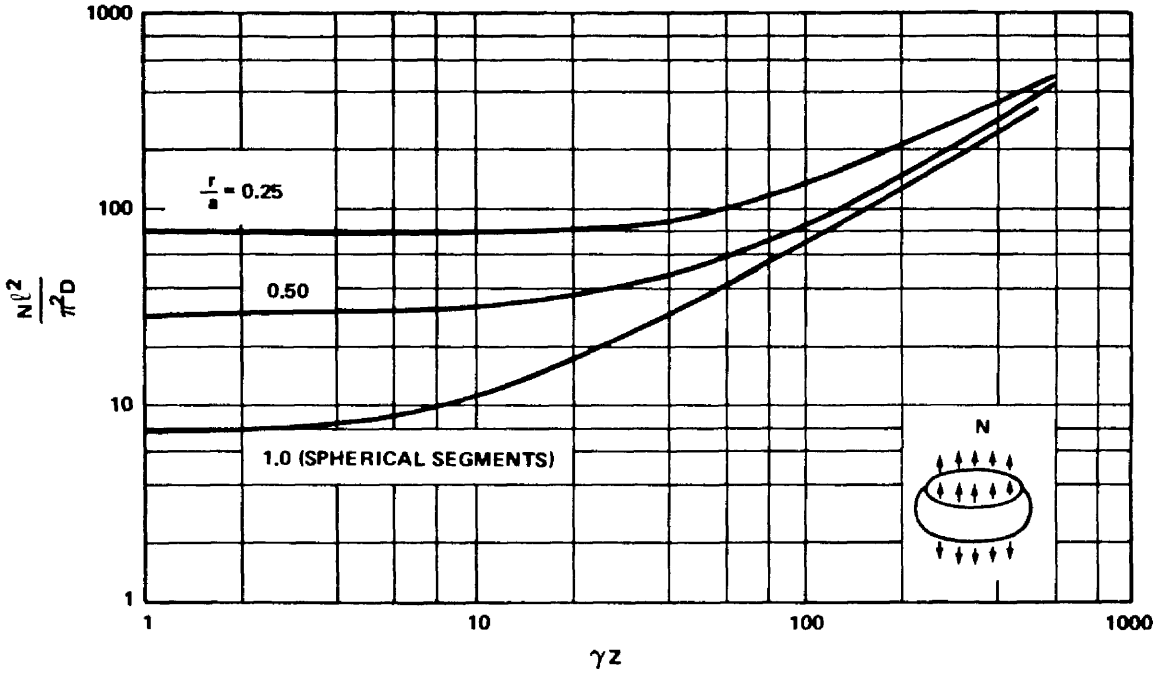

FIGURE 3.3-15. BUCKLING OF BOWED-OUT TOROIDAL SEGMENTS UNDER AXIAL TENSION

$$\frac{N\ell^2}{\pi^2 D} = \frac{1}{\left(\frac{r}{a}\beta^2 - 1\right)} \left[(1+\beta^2)^2 + 12 \frac{\gamma^2 Z^2}{\pi^4} \left(\frac{1 + \frac{r}{a}\beta^2}{1+\beta^2} \right)^2 \right] \qquad (9)$$

where the correlation coefficient γ has been inserted to account for discrepancies between theory and experiment. The values obtained by minimizing equation (9) with respect to β are shown in Figure 3.3-15. The straight-line portion of the curves is represented by the relationship

$$\frac{N\ell^2}{\pi^2 D} = \frac{4\sqrt{3}}{\pi^2} \gamma Z \qquad (10)$$

A similar analytical investigation described in Reference 30 for clamped truncated hemispheres in axial tension yields results in close agreement with those for the curve of Figure 3.3-15 for $r/a = 1$.

The experimental results for the truncated hemisphere given in Reference 30 indicate that the correlation coefficient for the curve for r/a equals 1 is

$$\gamma = 0.35 \quad . \tag{11}$$

The same value of the correlation coefficient may be used for other values of r/a.

Some results for bowed-out equatorial toroidal segments under axial compression are given in Reference 31; the equatorial spherical shell segment loaded by its own weight is treated in Reference 32.

3.3.1.9 Shallow Toroidal Segments Under External Pressure.

The term "lateral pressure" designates an external pressure which acts only on the curved walls of the shell and not on the ends; "hydrostatic pressure" designates an external pressure that acts on both the curved walls and the ends of the shell. Expressions for simply supported shallow equatorial toroidal segments subjected to uniform external lateral or hydrostatic pressure (Figs. 3.3-16 and 3.3-17) are given in Reference 33 as

$$\frac{P_{cr}\, r\ell^2}{\pi^2 D} = \frac{1}{\beta^2}\left[(1+\beta^2)^2 + \frac{12}{\pi^4}\gamma^2 Z^2 \left(\frac{1 \pm \frac{r}{a}\beta^2}{1+\beta^2}\right)^2\right] \tag{12}$$

for lateral pressure, and as

$$\frac{P_{cr}\, r_\ell^2}{\pi^2 D} = \frac{1}{\beta^2\left(1 \mp 1/2\,\frac{r}{a}\right) + 1/2}\left[(1+\beta^2)^2 + \frac{12}{\pi^4}\gamma^2 Z^2 \left(\frac{1 \pm \frac{r}{a}\beta^2}{1+\beta^2}\right)^2\right] \tag{13}$$

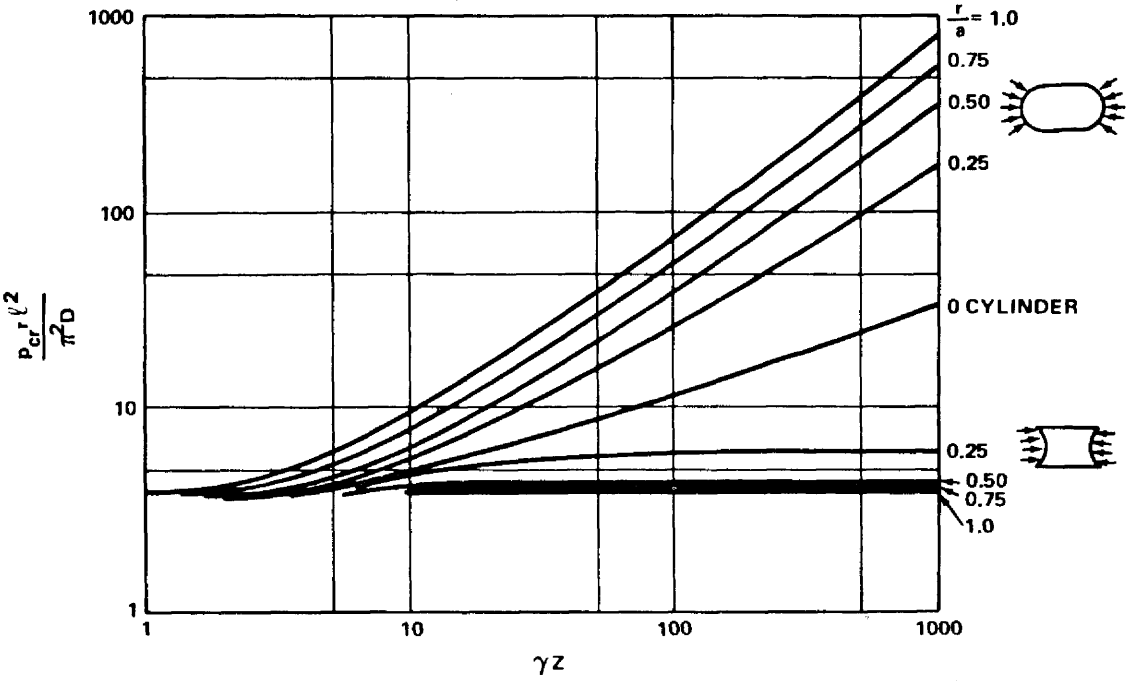

FIGURE 3.3-16. BUCKLING OF TOROIDAL SEGMENTS UNDER UNIFORM LATERAL PRESSURE

for hydrostatic pressure. In equations (12) and (13), the upper sign refers to segments of type (a) of Figure 3.3-18, whereas the lower sign refers to segments of type (b) of Figure 3.3-18. The correlation coefficient γ has been introduced to account for discrepancies between theory and experiment. The results of minimizing the buckling pressure with respect to the circumferential wavelength parameter β are shown in Figures 3.3-16 and 3.3-17. The straight-line portions of the curve for the shells of type (a) of Figure 3.3-18 are represented by the relationships

$$\frac{P_{cr} r_\ell^2}{\pi^2 D} = \frac{4\sqrt{3}}{2} \frac{r}{a} \gamma Z \qquad \text{(lateral pressure)} \quad . \qquad (14a)$$

$$\frac{P_{cr} r_\ell^2}{\pi^2 D} = \frac{8\sqrt{3}}{2 - \frac{r}{a}} \frac{r}{a} \gamma Z \qquad \text{(hydrostatic pressure)} \quad . \qquad (14b)$$

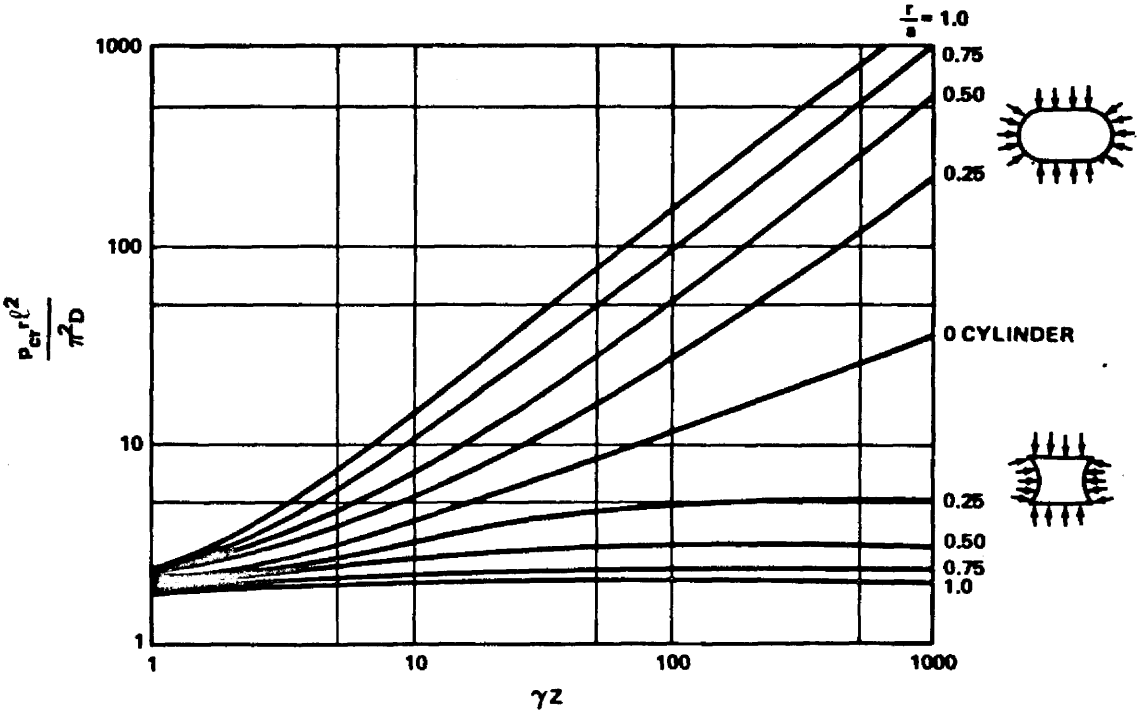

FIGURE 3.3-17. BUCKLING OF TOROIDAL SEGMENTS UNDER UNIFORM EXTERNAL HYDROSTATIC PRESSURE

No experimental data are available except for the cylindrical shell, for which a correlation factor of

$$\gamma = 0.56 \tag{15}$$

was recommended in Reference 28. The same correlation factor can be used for shells with r/a near zero but should be used with caution for shells of type (b) with values of r/a near unity. For shells of type (a) with values of r/a near unity, the shell can be conservatively treated as a sphere, or the buckling pressure should be verified by test.

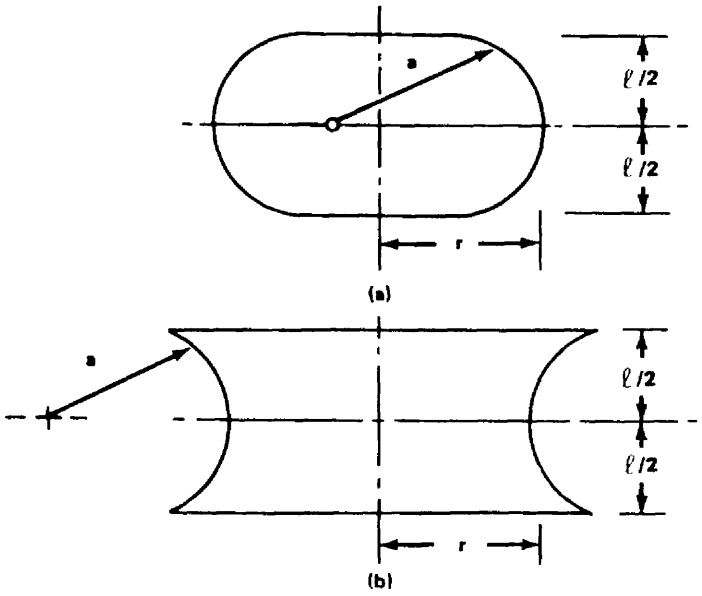

FIGURE 3.3-18. GEOMETRY OF TOROIDAL SEGMENTS NEAR EQUATORS

3.3.2 ORTHOTROPIC DOUBLY CURVED SHELLS.

The term "orthotropic doubly curved shells" covers a wide variety of shells. In its strictest sense, it denotes single- or multiple-layered shells made of orthotropic materials. In this section, the directions of the axes of orthotropy for shells of revolution are assumed to coincide with the meridional and circumferential directions of the shell. The term also denotes types of stiffened shells in which the stiffener spacing is small enough for the shell to be approximated by a fictitious sheet whose orthotropic bending and extensional properties include those of the individual stiffening elements averaged out over representative widths or areas.

The behavior of the various types of orthotropic shells may be described by a single theory, the governing equations of which are equations of equilibrium for the buckled structure, and relationships between force and

moment resultants and extensional and bending strains. The matrix equation relating the inplane forces and bending moments to the inplane strains and curvatures for shells of revolution with axes of orthotropy in the meridional and circumferential directions can be written in the following form:

$$\begin{Bmatrix} N_1 \\ N_2 \\ N_{12} \\ M_1 \\ M_2 \\ M_{12} \end{Bmatrix} = \begin{bmatrix} C_{11} & C_{12} & 0 & C_{14} & C_{15} & 0 \\ C_{12} & C_{22} & 0 & C_{24} & C_{25} & 0 \\ 0 & 0 & C_{33} & 0 & 0 & 0 \\ C_{14} & C_{24} & 0 & C_{44} & C_{45} & 0 \\ C_{15} & C_{25} & 0 & C_{45} & C_{55} & 0 \\ 0 & 0 & 0 & 0 & 0 & C_{66} \end{bmatrix} \begin{Bmatrix} \epsilon_1 \\ \epsilon_2 \\ \epsilon_{12} \\ \kappa_1 \\ \kappa_2 \\ \kappa_{12} \end{Bmatrix} \tag{16}$$

Zero entries in the preceding matrix generally refer to coupling terms for layers whose individual principal axes of stiffnesses are not aligned in meridional and circumferential directions. The values of the various elastic constants used in determining buckling loads of orthotropic shells are different for different types of construction. Some widely used expressions are given in References 1 and 34.

The theory for single-layered shells of orthotropic material is similar to that for isotropic shells since the coupling terms C_{14}, C_{15}, C_{24}, and C_{25} may be set equal to zero. For stiffened doubly curved shells or for shells having multiple orthotropic layers, this is not generally possible, and it is shown in References 35 and 36 that the neglect of coupling terms can lead to serious errors. For example, the inclusion of coupling terms yields a significant difference in theoretical results for stiffened shallow spherical-dome configurations having stiffeners on the inner surface or on the outer surface. The difference vanishes when coupling is neglected.

Very little theoretical or experimental data are available for orthotropic and stiffened doubly curved shells. The general instability loads of pressurized shallow spherical domes with meridional stiffeners are determined in Reference 37, and a semiempirical design formula is given in Reference 38 for stiffened spherical caps. This formula closely approximates the test data given in Reference 38. Buckling loads are given for grid-stiffened spherical domes in Reference 39. References 37 and 39 do not include the effect of stiffener eccentricity.

Stiffener-eccentricity effects are investigated in Reference 35 for grid-stiffened spherical domes. Eccentrically stiffened shallow equatorial toroidal shells under axial load and uniform pressure are investigated in Reference 40. The development of a buckling computer program that includes coupling as well as nonlinear prebuckling bending effects for orthotropic shells of revolution is discussed in References 1 and 34. A further description of this program is given in Subsection 3.4. (The cards and a computer listing for this program are available from COSMIC, University of Georgia, Athens, Ga.) Numerical results obtained from this program [34] were in good agreement with selected experimental results. The computer program can be used to determine the buckling load of the following orthotropic shells:

1. Shells with ring and stringer stiffening.
2. Shells with skew stiffeners.
3. Fiber-reinforced (layered) shells.
4. Layered shells (isotropic or orthotropic).
5. Corrugated ring-stiffened shells.
6. Shells with one corrugated and one smooth skin (with rings).

Boundary conditions may be closed at one or both ends or may be free, fixed, or elastically restrained. Edge rings are permitted on the boundary or as discrete rings in the shell.

This computer program can be used in conjunction with experimentally determined correlation factors to obtain buckling loads for orthotropic shells of revolution. The limitations of the program are given in References 1 and 34 and are also discussed in Subsection 3.4.

The design recommendations that follow are limited to spherical domes; the recommendations should also be verified by test, where feasible. The possibility of local buckling of the shell between stiffening elements should be checked.

The investigation of Reference 39 gives the theoretical buckling pressure of a grid-stiffened spherical dome under uniform external pressure. This analysis assumes that the spherical dome is "deep" and that it contains many buckle wavelengths. In this case, the boundary conditions have little effect on the buckling load. Eccentricity effects are neglected. Experimental results given in Reference 24 tend to support the assumptions of the analysis.

If the analysis of Reference 39 is extended to the materially or geometrically orthotropic shell, the hydrostatic buckling pressure can be expressed as

$$\frac{pr^3}{C_{44}\,\psi_1^{1/2}} = 4\gamma\left(\frac{1 + 2\,\frac{C_{45} + C_{66}}{C_{44}} + \frac{C_{55}}{C_{44}}}{1 + \frac{C_{22}}{C_{11}} + 2\,\frac{C_{22}}{\psi_2}}\right)^{1/2} \qquad (17)$$

where

$$\psi_1 = \frac{C_{22}\,r^2}{C_{44}}\left(1 - \frac{C_{22}^2}{C_{11}\,C_{22}}\right) \quad , \qquad (18a)$$

$$\psi_2 = \frac{2\,C_{33}}{1 - \frac{C_{12}^2}{C_{11}\,C_{22}} - 2\,\frac{C_{12}\,C_{33}}{C_{11}\,C_{22}}} \quad . \qquad (18b)$$

The constants C_{11} , C_{12} , C_{22} , C_{33} , C_{44} , C_{45} , C_{55} , and C_{66} are defined in Reference 34 for the various materially and geometrically orthotropic materials. Equation (17) does not include the effect of stiffener eccentricity since the coupling terms C_{14} , C_{15} , C_{24} , and C_{25} in equation (16) have been neglected. Only limited experimental data exist for geometrically or materially orthotropic spherical domes subjected to hydrostatic pressure [24, 38]. In the absence of more extensive test results, it is recommended that the isotropic spherical cap reduction factor shown in equation (4) also be used for the orthotropic spherical shell. The correlation factor is given by

$$\gamma = 0.14 + \frac{3.2}{\lambda^2} \quad . \qquad (19)$$

Refer to Figure 3.3-2 for the plot of this equation. The effective shell thickness to be used in obtaining λ is recommended as

$$t = \sqrt[4]{\frac{C_{44}\,C_{55}}{C_{11}\,C_{22}}}\;\sqrt{12} \quad . \qquad (20)$$

3.3.3 ISOTROPIC SANDWICH DOUBLY CURVED SHELLS.

The term "isotropic sandwich" designates a layered construction formed by bonding two thin isotropic facings to a thick core. Generally, the thin isotropic facings provide nearly all the bending rigidity of the construction. The core separates the facings and transmits shear so that the facings bend about a common neutral axis.

Sandwich construction should be checked for two possible modes of instability failure: (1) general instability failure where the shell fails with core and facings acting together, and (2) local instability failure taking the form of dimpling of the faces or wrinkling of the faces (Fig. 3.1-7).

3.3.3.1 General Failure.

If the sandwich core is resistant to transverse shear so that its shear stiffness can be assumed to be infinite, the sandwich shell can be treated as an equivalent isotropic shell. For unequal thickness facings, the equivalent isotropic material thickness and modulus of elasticity are then given by

$$\bar{t} = \frac{\sqrt{12}\, h}{\sqrt{\frac{E_1 t_1}{E_2 t_2}} + \sqrt{\frac{E_2 t_2}{E_1 t_1}}} \quad , \tag{21a}$$

$$\bar{E} = \frac{E_1 t_1 + E_2 t_2}{\bar{t}} \tag{21b}$$

and for equal-thickness facings with the same modulus of elasticity, by

$$\bar{t} = \sqrt{3}\, h \quad , \tag{22a}$$

$$\bar{E} = \frac{2 E t_f}{\sqrt{3}\, h} \quad . \tag{22b}$$

These equivalent properties can be used in conjunction with the recommended practices in Paragraph 3.3.1 and with the computer program of Reference 34 to analyze isotropic sandwich doubly curved shells.

Only one theoretical investigation which includes shear flexibility is available. In Reference 41 the buckling of a sandwich sphere comprised of a core layer of low-modulus material and two equal face layers of high-modulus material is discussed. Because there are insufficient theoretical and experimental data, no design recommendations can be given for this case.

3.3.3.2 Local Failure.

Modes of failure other than overall buckling are possible. For honeycomb-core sandwich shells, failure may occur because of core crushing, intracell buckling, and face wrinkling. The use of relatively heavy cores ($\delta > 0.03$) will usually prevent core crushing. Lighter cores may prove to be justified as data become available. Procedures for the determination of intracell buckling and face-wrinkling loads are given in Reference 42.